Energy Storage Materials 50 (2022) 380–386

Contents lists available at ScienceDirect

Energy Storage Materials

journal homepage: www.elsevier.com/locate/ensm

Achieving high-energy-density magnesium/sulfur battery via a passivation-free Mg-Li alloy anode

Ruinan Li, Qingsong Liu, Rupeng Zhang, Yaqi Li, Yulin Ma, Hua Huo, Yunzhi Gao, Pengjian Zuo *, Jiajun Wang *, Geping Yin *

MIIT Key Laboratory of Critical Materials Technology for New Energy Conversion and Storage, School of Chemistry and Chemical Engineering, Harbin Institute of Technology, Harbin 150001, Heilongjiang, China

ARTICLE INFO

Keywords:
Magnesium-sulfur batteries
magnesium anode
magnesium alloy
passivation
overpotential
energy density

ABSTRACT

Magnesium/sulfur batteries have emerged as one of the considerable choices for next-generation batteries. However, its low voltage platform caused by the passivation of magnesium anode limits its actual energy density. Herein, a magnesium-lithium alloy is screened out as a passivation-free anode, which hinders the passivation reaction on the anode through the substitution reaction between lithium in the alloy and the magnesium ions in the electrolyte. The alloy anode exhibits an improved interfacial reaction kinetics, and the impedance is reduced by 5 orders of magnitude compared to that of magnesium anode. With passivation-free Mg-Li alloy anode, the magnesium/sulfur battery achieves an enhanced discharge voltage platform of 1.5 V and an energy density of 1829 Wh kg^{-1}. This study provides a novel design of passivation-free magnesium alloy anode for high-energy-density magnesium/sulfur batteries.

1. Introduction

Lithium-sulfur battery is considered as one of the most attractive battery systems with high-energy density due to its ultra-high specific capacity of 1675 mAh g^{-1}, low cost, and environmental friendliness. However, lithium dendrites pose a safety risk, limiting their practical application. Magnesium, on the other hand, is a suitable anode material with a low reduction potential of -2.37 V (vs. SHE) and a high volumetric capacity of 3837 mAh cm^{-3} (almost twice that of lithium which is 2062 mAh cm^{-3}) [1,2]. Besides, dendrites rarely grow on their surface, which is the distinct advantage of Mg anode over other common metal anode candidates [3,4]. Therefore, magnesium/sulfur batteries have emerged as a promising option for next-generation batteries. However, different from lithium anode, the surface film generated by the chemical reaction between Mg anode and most conventional anions in an electrolyte (such as ClO_4^-, PF_6^- and BF_4^-) cannot conduct Mg^{2+} [1,5], which leads to the passivation of Mg anode. As a result, the overpotential of the Mg anode increases dramatically during cycling, causing a low discharge voltage platform and the consequent low energy density of the Mg/S batteries.

One approach to address the issue of Mg anode passivation is to develop electrolytes that do not react with magnesium to form a passivation film. Aurbach et al. proposed the Grignard reagent (RMgX, R=alkyl or aryl group, X=halogen) electrolyte [6] and the all phenyl complex (APC) electrolyte [7] that enable the reversible deposition and dissolution of Mg. However, both electrolytes are incompatible with the electrophilic sulfur cathodes due to their nucleophilicity. A non-nucleophilic electrolyte prepared by adding HMDSMgCl and $AlCl_3$ to THF was firstly proposed in 2011 [8], while this electrolyte is sensitive to humidity and air, poor in oxidation stability, and corrosive to current collectors [9].

Another method to avoid the passivation of Mg anode is to tailor a solid electrolyte interphase (SEI) on the surface of Mg anode to allow the migration of Mg^{2+}. The surface film containing MgF_2 and MgI_2 on the Mg anode has been confirmed to act as SEI. [10,11]. Some novel electrolytes including magnesium-aluminum chloride complex (MACC) electrolytes [12–14] and organoborane-based electrolytes [15–22], as well as electrolyte additives such as $MgCl_2$ [23,24], LiCl [25] and ionic liquids [13,26,27], were developed and proved to form SEI on Mg anode surface. Nevertheless, the introduced halogen ions in electrolytes could cause severe corrosion of current collectors and inert components in the batteries. Furthermore, 'artificial SEI' was achieved on the magnesium surface which can protect magnesium anode from block [28,29]. Whereas, these 'artificial SEI' are either complicated to fabricate or not stable enough in long-term cycling.

* Corresponding authors.
E-mail addresses: zuopj@hit.edu.cn (P. Zuo), jiajunhit@hit.edu.cn (J. Wang), yingphit@hit.edu.cn (G. Yin).

https://doi.org/10.1016/j.ensm.2022.05.039
Received 6 February 2022; Received in revised form 23 April 2022; Accepted 22 May 2022
Available online 24 May 2022

Herein, a novel strategy is proposed to suppress the passivation of magnesium anode. Magnesium-lithium alloy is employed as the anode material to enable the substitution reaction between the lithium in the alloy and the magnesium ions in the $Mg(TFSI)_2$/DME electrolyte, which hinders the passivation reaction on the anode surface. As a consequence, the surface film impedance of the resultant Mg-Li/S battery is five orders of magnitude lower than that of the Mg/S battery, demonstrating an improved electrochemical activity. In addition, the discharge voltage platform and energy density of the Mg-Li/S battery increase to 1.5 V and 1829 Wh kg^{-1} respectively, compared with the 0.3 V and 287 Wh kg^{-1} of Mg/S battery. With the combination of X-ray tomography, X-ray photoelectron spectroscopy (XPS), and attenuated total reflection Fourier transform infrared spectroscopy (ATR-FTIR) analysis, it was revealed that the majority of Mg and a small amount of Li are engaged in the anode electrochemical process. This study offers a feasible passivation-free anode to achieve a high discharge voltage platform and high energy density for magnesium/sulfur batteries.

2. Results and discussion

2.1. Design principles and physical characterizations

The displacement reaction on the surface of the magnesium anode may result in an active anode/electrolyte interface, which can hinder the passivation reaction [31]. Alloying magnesium is a straightforward and practical way to achieve a substitution process between the magnesium anode and the electrolyte. A passivation-free magnesium alloy material usually complies with the following two principles: (i) The standard electrode potential of alloyed metals should be lower than that of Mg (-2.37 V vs. SHE) to trigger the substitution reaction between the magnesium alloy and the electrolyte containing only Mg^{2+} cations. (ii) The selected alloyed metal should have a low relative atomic mass and have a negligible effect on the high theoretical specific capacity of the anode. Fig. 1a shows the standard electrode potential and relative atomic mass of the common magnesium alloy components. Among these elements, only the standard electrode potential of Li and Ca fulfill the criterion. As a result of its low standard electrode potential and relative atomic mass, lithium becomes an ideal alloying material. In addition, the as-formed Mg-Li alloy is economical, easy-to-obtain, and privileged in terms of plasticity and rigidity. As a consequence, a Mg-Li alloy material composed of 90 wt.% magnesium, 9 wt.% lithium, and 1 wt.% zinc is selected here. The inductively coupled plasma-optical emission spectrometry (ICP) was carried out to demonstrate its components (Tab. S1).

The composition ratio of the Mg-Li alloy is designed to allow the two phases to coexist in the alloy material. The alloy contains both α phase with a close-packed hexagonal crystal structure and β phase with a body-

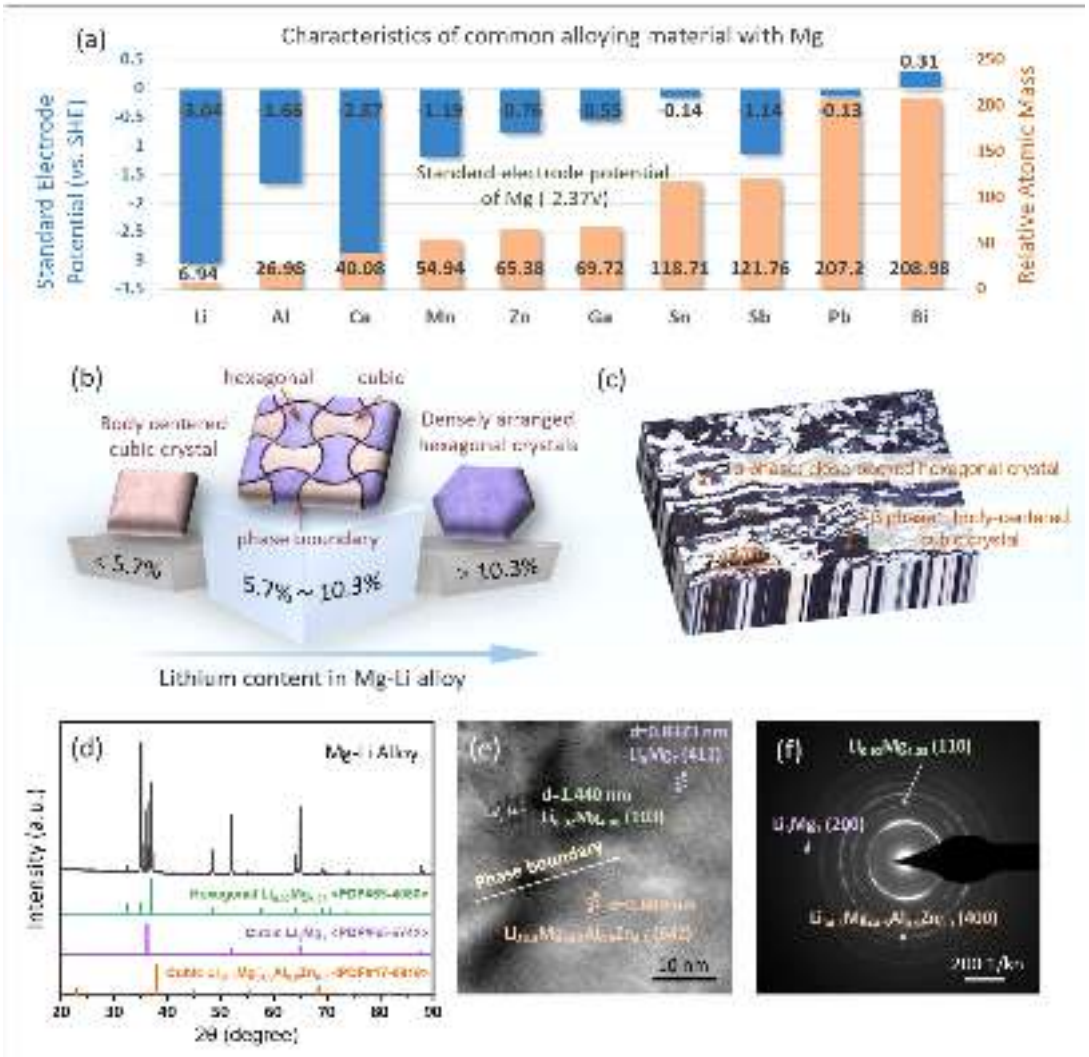

Fig. 1. Physical characterizations of the selected Mg-Li alloy. (a) Standard electrode potential and relative atomic mass of the common alloy materials with Mg. (b) Schematic of the phase structures of Mg-Li alloy with different Li contents. (c) OM, (d) XRD pattern, (e) HRTEM image, and (f) Electron diffraction pattern of the Mg-Li alloy.

centered cubic crystal structure when the lithium concentration is 9 wt. % (Fig. 1b). The abundant phase boundaries of the alloy can be observed through an optical micrograph (OM) (Fig. 1c), after being etched by the etching solution (see SI for details). The lighter area in the OM is the α phase and the dark area is the β phase, and the phase boundaries have been proved to accelerate Mg^{2+} ion transport and improve its electrochemical performance [30]. Therein, the small amount of Zn can act as an inert component. Fig. 1d depicts the XRD pattern of the Mg-Li alloy. The diffraction peaks correspond well with hexagonal $Li_{0.92}Mg_{4.08}$ (PDF#65-4080), cubic Li_3Mg_7 (PDF#65-6742), and cubic $Li_{34.3}Mg_{64.5}Al_{0.9}Zn_{0.3}$ (PDF#17-0919). Furthermore, the two phases and phase boundaries can be observed in the HRTEM image and the electron diffraction pattern (Fig. 1e, f). The lattice fringes with the spacings of 0.8373 nm, 1.440 nm, and 0.889 nm correspond to the (411) crystal plane of Li_3Mg_7, the (103) crystal plane of $Li_{0.92}Mg_{4.08}$, and the (642) crystal plane of $Li_{34.3}Mg_{64.5}Al_{0.9}Zn_{0.3}$ respectively, and the diffraction rings of (200) crystal plane of Li_3Mg_7, the (110) crystal plane of $Li_{0.92}Mg_{4.08}$, and the (400) crystal plane of $Li_{34.3}Mg_{64.5}Al_{0.9}Zn_{0.3}$ are observed in the electron diffraction pattern. The HRTEM results correspond well with the XRD result.

The stability of the Mg-Li alloy was tested by exposing it to air for 10 days and water for 48 hours (Fig. S1). The surface of the Mg-Li alloy foil soaked in water turns black, while there is no apparent change of the Mg-Li alloy which has been exposed to the air, indicating that the stability of Mg-Li alloy is comparative to pure Mg metal and in sharp contrast to Li metal (Tab. S2). Therefore, the lithium in the Mg-Li alloy has almost no negative effect on the inherent stability of the Mg-Li/S battery.

2.2. Electrochemical performance

Galvanostatic discharge/charge tests of Mg-Li/S battery and Mg/S battery with 0.5 M $Mg(TFSI)_2$/DME electrolyte were represented in Fig. 2a. The discharge profile of Mg/S battery exhibits a voltage hysteresis process in which the initial voltage platform is approximately 0.3 V and then the voltage increases to about 0.8 V, which is attributed to the initial passivation state of the Mg anode surface [31]. In contrast, the discharge voltage platform of the Mg-Li/S battery maintains as high as 1.5 V without a voltage hysteresis, indicating a lower overpotential of Mg-Li anode compared to that of Mg anode. The improved discharge voltage enables the energy density of the Mg-Li/S battery up to 1829 Wh kg^{-1} compared to 287 Wh kg^{-1} of the Mg/S battery, which is calculated based on the mass of cathode active material (sulfur). In addition, the Mg-Li/S battery can maintain a high discharge voltage during subsequent cycles, whereas the Mg/S battery has almost no reversible capacity (Fig. 2b). Symmetric batteries were taken to evaluate the overpotential of Mg-Li alloy and Mg electrode (Fig. S2). As displayed in the voltage profiles, the overpotential of an Mg-Li alloy symmetric battery is lower than that of an Mg symmetric battery after several initial cycles of instability, and the cycling can last 400 times. Fig. 2c and 2d depict the surface morphology of Mg-Li alloy anode after the battery has been cycled. Different from the dendritic morphology of lithium, hexagonal stripping holes and spherical deposits are observed, which are the characteristics of magnesium stripping and deposition [32]. A small amount of Li in the Mg-Li alloy anode has no effect on the anode deposition morphology during the battery charging and hence avoids the risk of a battery short circuit.

Electrochemical impedance spectroscopy (EIS) measurements are employed for the Mg-Li/S and Mg/S batteries (Fig. 2e). The equivalent circuits are illustrated in the insets, and the detailed fitting results are

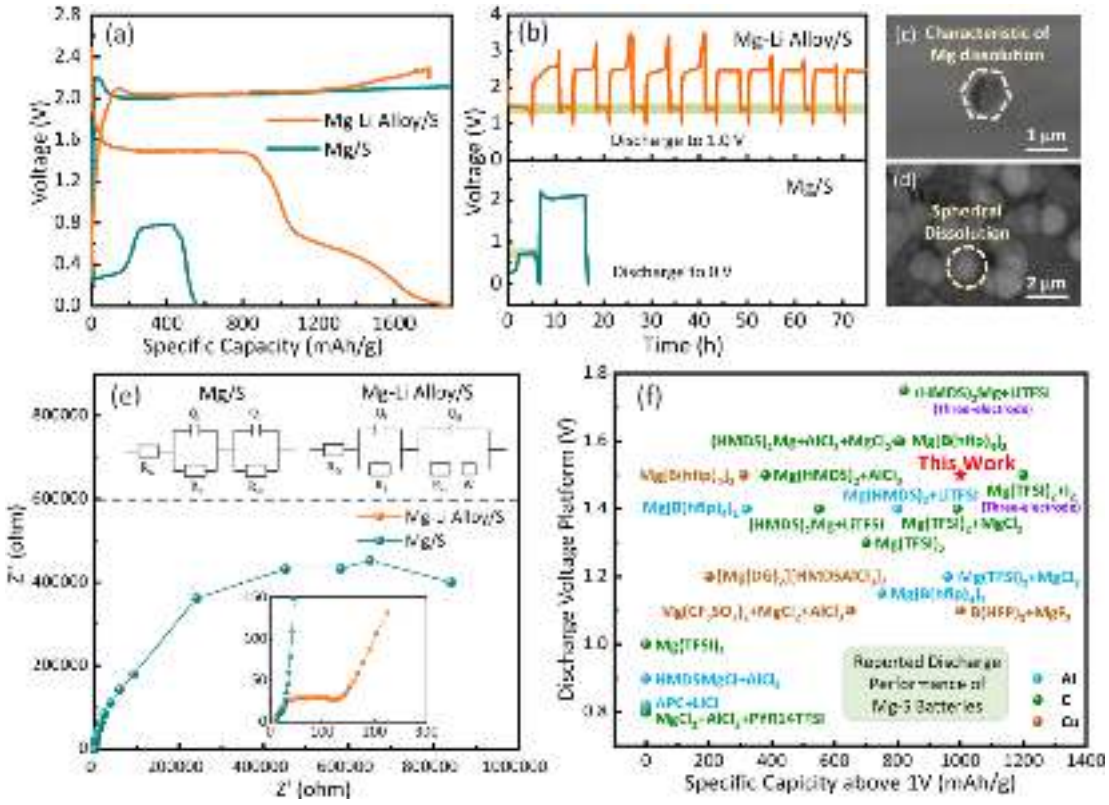

Fig. 2. Electrochemical performance of the Mg-Li alloy anode. (a) First discharge/charge curves and (b) Discharge/charge profiles of Mg-Li/S battery and Mg/S battery with 0.5 M $Mg(TFSI)_2$ electrolyte at 0.05 C. SEM images of Mg-Li alloy anode (c) after first discharge and (d) after 5 discharge/charge cycles. (e) EIS of Mg-Li/S battery and Mg/S battery. Insets show the equivalent circuits of the two batteries and the zoom-in region of EIS. (f) The voltage-capacity plots of newly reported works [8,11, 13-18, 21,22, 24-27, 33-47].

given in Tab. S3. Ohmic resistances, interfacial impedance, and charge transfer impedance are denoted by R_Ω, R_I, and R_{ct}, respectively. According to the fitting results, the R_I of Mg-Li/S battery is 4.594 Ω, whereas the R_I of Mg/S battery is as high as 970400 Ω, which is over five orders of magnitude greater than that of Mg-Li/S battery. The ultra-high R_I reflects the poor interfacial reaction kinetics, which blocks Mg^{2+} ions from passing through the surface film on Mg anode. Mg-Li alloy, on the other hand, can function as a passivation-free anode, resulting in a low interfacial impedance, which can be identified as R_{SEI}.

The discharge performance of the Mg-Li/S battery here is compared with that of newly reported Mg/S batteries (Fig. 2f), and only the specific capacity with voltage greater than 1V is counted. Compared to the two-electrode cell, the Mg/S batteries tested with the three-electrode cell show a higher voltage plateau because the effect of anode overpotential is excluded. Among all two-electrode systems, the battery system in this work presents optimal discharge voltage platform and specific capacity, resulting in an ultra-high energy density, especially when compared to the Mg/S batteries with the same $Mg(TFSI)_2$ electrolyte and the batteries with Al cathode current collector.

2.3. Analysis of the electrochemical behavior of Mg-Li alloy anode

X-ray tomography was employed to reveal the change of the 3D microstructure of Mg-Li alloy (Fig. 3a, b) and Mg anode (Fig. 3d, e) surface after stripping. Different from the Mg metal, the pristine Mg-Li alloy is spongy, and the holes correspond to Li because of its weak absorptivity. After the Mg-Li alloy is stripped, the surface becomes uneven, demonstrating the existence of stripping holes. Besides, the cut-view (inset of Fig. 3b) shows the distribution of the holes (the black area), indicating that the small holes are densely distributed on the alloy anode after stripping. These results prove a structural stripping of Mg and exclude the possibility that Mg is only used as a skeleton. To further analyze the difference in morphology, regions of the same size were intercepted on the alloy anode surface before and after stripping, to compare the value of their superficial area (Fig. 3c). The results demonstrate the increase in the superficial area of the alloy after stripping, resulting from a large number of stripping holes. In contrast, for Mg anode, larger stripping holes are unevenly distributed after stripping, which is observed in Fig. 3e and the inset. This difference is also reflected in the SEM images (Fig. 3f, g). The stripping holes on Mg-Li alloy electrode are small and homogeneously distributed, indicating an improved interfacial reaction kinetics and homogeneous stripping. However, incomplete passivation causes large stripping holes on the Mg electrode surface and only a portion of the surface gets stripped, which is unfavorable for the cycle performance of the battery.

The electrochemical behavior of Mg, Li, and Zn in the alloy during battery cycling is investigated. X-ray photoelectron spectroscopy spectra (XPS) were performed to detect the cathode discharge products of the Mg-Li/S battery (Fig. 4a-c). The peak at around 50.0 eV in the Mg 2p spectrum corresponds to magnesium polysulfides (MgS_x) and MgS [34]. Correspondingly, in the S 2p spectrum, the peaks at 164.9 eV and 163.7 eV correspond to S^0 and MgS_x, and the peaks at 163.4 eV and 162.2 eV correspond to MgS [48]. On the contrary, the peak corresponding to Li 1s is not detected at 53.6~57.2 eV, which might be owing to the extremely low lithium concentration/content in the cathode discharging products or the high solubility of lithium polysulfides in the electrolyte. Besides, there is no peak in Zn 2p spectrum, illustrating the absence of Zn stripping during the battery discharge. The full XPS spectrum and high-resolution spectra of C 1s, O 1s, F 1s and N 1s are given in Fig. S3 and S4.

The ICP results (Fig. 4d) manifest that after the first discharge of Mg-Li/S battery, a small amount of Li^+ is detected in electrolyte and cathode for 0.4% and 2.8% respectively, and no Zn^{2+} is detected. The calculation results (see supporting information for details) reveals that the total quantity of lithium in the KB/S cathode and electrolyte is 3.76×10^{-3} mmol after the discharging of the Mg-Li/S battery. If the capacity of this battery is all achieved by the migration of Li^+, the amount of Li^+ stripped from Mg-Li alloy anode is calculated to be 2.6×10^{-2} mmol. Consequently, the number of charges provided by Li^+ accounts for only 14.45% of the total number of transferred charges. According to the ICP results and XPS results, the oxidation reactions on Mg-Li alloy anode are proceeded by the co-electrochemical stripping of both Mg^{2+} and Li^+, and Mg stripping is dominant (85.55%). The corresponding schematic of the stripping process is exhibited in Fig. 4e.

2.4. Mechanism analysis

To investigate the mechanism of the Mg-Li alloy avoiding passivation, the variations of EIS with the standing time for Mg-Li/S battery and Mg/S battery were employed (Fig. 5a, b) and the detailed fitting

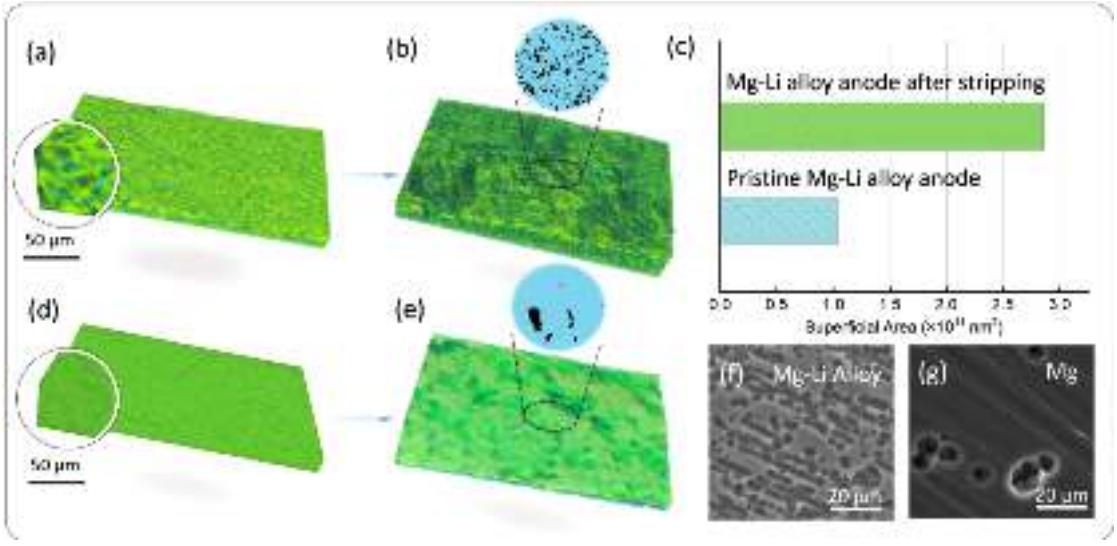

Fig. 3. Comparison of the discharge process of Mg-Li alloy anode and Mg anode. X-ray tomography of the surface of (a) the pristine Mg-Li alloy anode and (b) the Mg-Li alloy anode after stripping. Inset: Cut-away view. (c) Superficial area of the pristine Mg-Li alloy anode and the Mg-Li alloy anode after stripping. X-ray tomography of the surface of (d) the pristine Mg anode and (e) the Mg anode after stripping. Inset: Cut-away view. SEM images of the anodes of (f) symmetric Mg-Li battery and (g) symmetric Mg battery after stripping.

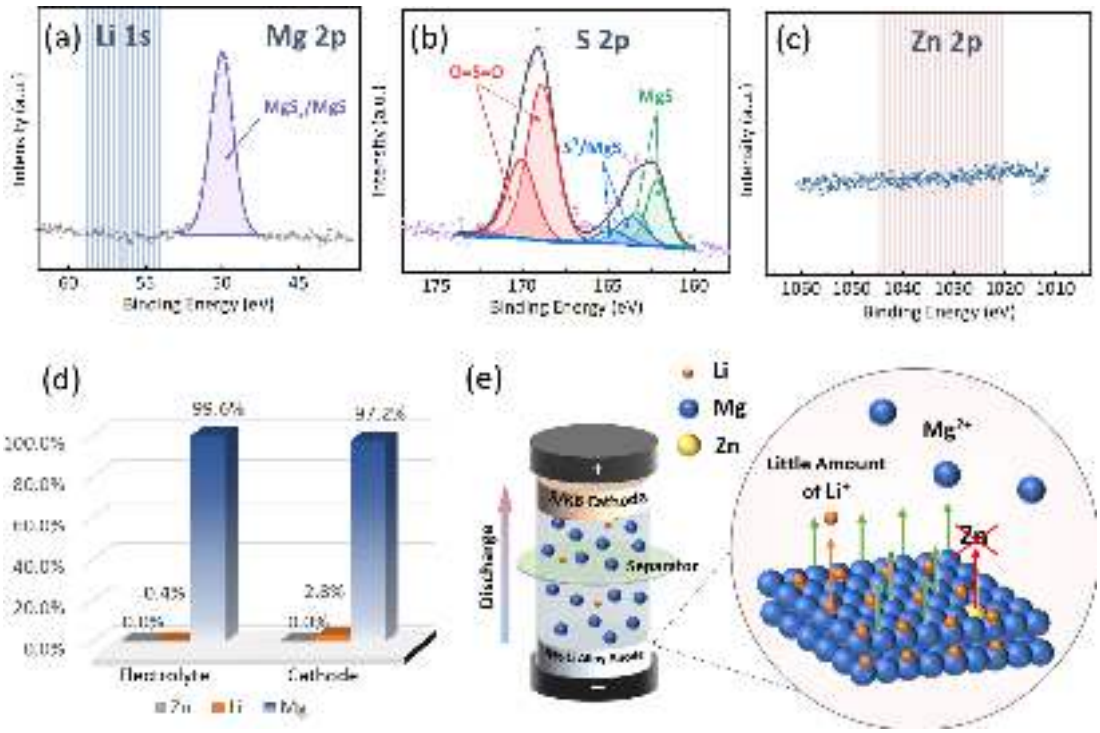

Fig. 4. Analysis of the discharge process of Mg-Li alloy anode. (a-c) XPS spectra of the KB/S cathode of Mg-Li/S battery after the first discharge. (d) ICP results of electrolyte and cathode of Mg-Li/S battery after the first discharge. (e) Schematic illustration of the stripping process of Mg-Li alloy anode.

results are given in Tab. S4 and S5. The EIS results reveal that the initial R_I of the Mg-Li/S battery is relatively low, illustrating its superior electrochemical activity. The impedance gradually increases as the battery standing time increases, indicating the gradual passivation of the Mg-Li alloy. While, Mg/S battery exhibits a relatively high R_I of approximately 10^6 Ω all the time, suggesting that Mg anode was passivated as soon as it exposes to the electrolyte. The differential changes of open-circuit voltage (OCV) for Mg-Li/S and Mg/S batteries further prove this result (Fig. 5c). Because of the Mg^{2+} insulated passive film on the Mg anode surface, the OCV of the Mg/S battery remains constant at around 1.0 V, which is much lower than the theoretical value. On the other hand, the initial OCV of the Mg-Li alloy/S battery is as high as 2.3 V but decreases rapidly to 1.48 V during the first 10 minutes, and then remains stable. The decrease of OCV corresponds to the gradual formation of the passive film on Mg-Li alloy anode surface, which is consistent with the results of EIS. It is worth noting that, the battery cannot achieve a high discharge voltage platform if the OCV of the Mg-Li/S batteries drops below 1.5 V, as the anode has been severely passivated. Therefore, the Mg-Li/S battery must be discharged within a window time of 10 min according to fig. 5c, or the Mg-Li alloy anode will be passivated, and the battery will not reach a discharge voltage platform as high as 1.5 V.

The passive film is observed on Mg anode surface after being briefly soaked in the electrolyte (Fig. 5d), and the passivated area corresponds to the intensive distribution of passive film content of S, F and O in the mapping results (Fig. 5h-j). However, there is no obvious change on Mg-Li alloy surface (Fig. 5e), and the C and O distribute uniformly on its surface (Fig. S5), which are likely introduced from the trace water and oxygen when preparing the samples and testing. The EDS results (Fig. 5f and Fig. S6) demonstrate that compared with Mg-Li alloy foil, Mg foil surface has a higher content of C, O, F, and S, which are the main components of passive film. Fig. 5k shows the FTIR results of Mg foil and Mg-Li alloy foil surface after soaked in electrolyte for 30 s. For the curve of Mg foil, the peak at 1192 cm^{-1} corresponds to vibration of SO_2 functional group; the peak at 1467 cm^{-1} corresponds to CH_2 or CH_3; the peak at 2855 cm^{-1} corresponds to CH_2 and the peak at 2928 cm^{-1} corresponds to CO_3 [49], which are the products of electrolyte decomposition. In contrast, only two small peaks at 2855 and 2928 cm^{-1} are observed for Mg-Li alloy. The above results indicate that when Mg foil is exposed to the electrolyte for a short period, the passive film forms immediately on Mg foil, whereas almost no passive film forms on Mg-Li alloy.

Based on the above analysis, the mechanism of the passivation-free Mg-Li alloy anode can be speculated. Fig. 5l demonstrates the anode/electrolyte interface after the Mg foil and the Mg-Li alloy are immersed in the electrolyte. A passive film forms immediately on the surface of the Mg anode due to the reduction of $TFSI^-$ anions, which does not allow Mg^{2+} anions to pass through and hinders the stripping of magnesium. In contrast, the passive film will not be formed immediately on the surface of the Mg-Li alloy anode. Since the ionic activity of Li^+ in the electrolyte is 0 and that in the Mg-Li alloy must be greater than 0, the chemical potential of Li in Mg-Li alloy is much greater than that in the electrolyte ($\mu_{Li_a} \gg \mu_{Li_s^+}$). As a result, the lithium in Mg-Li alloy migrates into the electrolyte, causing a substitution reaction as follows.

$$2Li_7Mg_{18} + 7Mg^{2+} \rightarrow 14Li^+ + 43Mg$$

This reaction causes a subsequent perturbance on the Mg-Li alloy anode/electrolyte interface and hinders the formation of the passive film. Therefore, the Mg-Li alloy anode is electrochemical active at this stage. However, as the substitution reaction reaches equilibrium, the chemical potential of Li in Mg-Li alloy equals that in the electrolyte ($\mu_{Li_a} = \mu_{Li_s^+}$), and as a result, the passivation gradually occurs. Because of the passivation film on the surface of the Mg-Li alloy anode, the electrochemical reaction cannot proceed at a low polarization after a period of time. In conclusion, Mg-Li alloy anode forms a passivation film in the electrolyte at a much slower rate than Mg anode.

3. Conclusion

In this work, to achieve a high-energy-density magnesium/sulfur battery, we have developed a novel strategy to address the challenge of

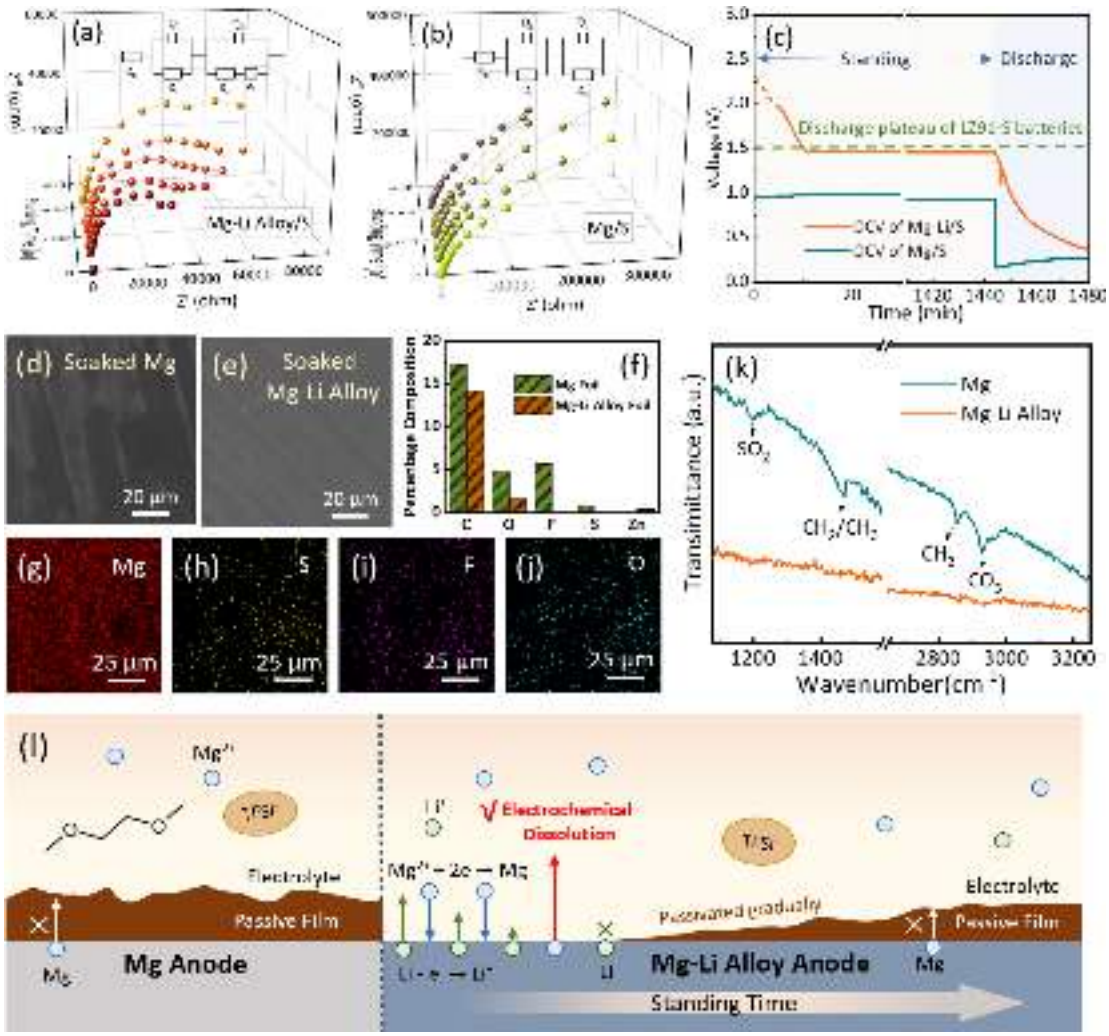

Fig. 5. Mechanism analysis of the passivation-free Mg-Li alloy anode. The changes of EIS with the storage time of (a) Mg-Li/S battery and (b) Mg/S battery. Insets show the equivalent circuits. (c) The changes of open-circuit voltage of Mg-Li/S battery and Mg/S battery. SEM images of (d) Mg foil and (e) Mg-Li alloy foil after soaking in the electrolyte for 30 s. (f) EDS results, (g-j) Mapping results, and (k) FTIR results of Mg foil and Mg-Li alloy foil after soaked in electrolyte for 30 s. (l) Schematic illustration of the passive film on Mg anode-electrolyte interface and the change of Mg-Li alloy anode/electrolyte interface withstanding time.

magnesium anode passivation by the interface reaction between the anode and the electrolyte. Mg-Li alloy is employed as a passivation-free anode material instead of the pure Mg metal, and the resulting Mg-Li alloy/S battery exhibits an enhanced discharge voltage platform of 1.5 V and an energy density of 1829 Wh kg^{-1}, which are superior to the control Mg-S battery sample in this study (0.3 V, 287 Wh kg^{-1}) and the currently reported Mg-S batteries. Besides, the surface film impedance of the Mg-Li/S battery is five orders of magnitude lower than that of Mg/S battery. During the electrochemical oxidation of the Mg-Li alloy anode, the vast majority of Mg and minority of Li are stripped, and the introduced lithium has almost no negative effect on battery safety. X-ray tomography, XPS, and ATR-FTIR were employed to study the mechanistic, and the results prove that the substitution reaction at the Mg-Li alloy anode/electrolyte interface hinders the formation of the passivation film, and as a result, the passivation speed of the Mg-Li alloy in the electrolyte is much slower than that of pure magnesium. This study provides a novel design of passivation-free magnesium alloy anode for high-energy-density Mg/S batteries.

Declaration of Competing interest

The authors declare that they have no known competing financial interests or personal relationships that could have appeared to influence the work reported in this paper.

Acknowledgments

This work was supported by National Natural Science Foundation of China (No. 22075063, No. U1932205), Chinesisch-Deutsches Mobilitätspropgamm (M-0281), Natural Science Funds of Heilongjiang Province (No. ZD2019B001), Heilongjiang Touyan Team (HITTY-20190033), the Fundamental Research Funds for the Central Universities" (Grant No. HIT.OCEF.2021028), Young Scientist Studio" of Harbin Institute of Technology (HIT), and funds from Chongqing Research Institute of HIT. We thank the beamline BL13W1 at Shanghai Synchrotron Radiation Facility (SSRF) for SR—CT measurements.

Supplementary materials

Supplementary material associated with this article can be found, in the online version, at doi:10.1016/j.ensm.2022.05.039.

Reference

[1] H.D. Yoo, I. Shterenberg, Y. Gofer, G. Gershinsky, N. Pour, D. Aurbach, Mg rechargeable batteries: an on-going challenge, Energ. Environ. Sci. 6 (2013) 2265–2279.

[2] P. Saha, M.K. Datta, O.I. Velikokhatnyi, A. Manivannan, D. Alman, P.N. Kumta, Rechargeable magnesium battery: Current status and key challenges for the future, Prog. Mater. Sci. 66 (2014) 1–86.
[3] C. Ling, D. Banerjee, M. Matsui, Study of the electrochemical deposition of Mg in the atomic level: Why it prefers the non-dendritic morphology, Electrochim. Acta 76 (2012) 270–274.
[4] M. Jackle, K. Helmbrecht, M. Smits, D. Stottmeister, A. Gross, Self-diffusion barriers: possible descriptors for dendrite growth in batteries? Energ. Environ. Sci. 11 (2018) 3400–3407.
[5] Z. Lu, A. Schechter, M. Moshkovich, D. Aurbach, On the electrochemical behavior of magnesium electrodes in polar aprotic electrolyte solutions, J. Electroanal. Chem. 466 (1999) 203–217.
[6] D. Aurbach, Z. Lu, A. Schechter, Y. Gofer, H. Gizbar, R. Turgeman, Y. Cohen, M. Moshkovich, E. Levi, Prototype systems for rechargeable magnesium batteries, Nature 407 (2000) 724.
[7] O. Mizrahi, N. Amir, E. Pollak, O. Chusid, V. Marks, H. Gottlieb, L. Larush, E. Zinigrad, D. Aurbach, Electrolyte solutions with a wide electrochemical window for recharge magnesium batteries, J. Electrochem. Soc. 155 (2008) A103–A109.
[8] H.S. Kim, T.S. Arthur, G.D. Allred, J. Zajicek, J.G. Newman, A.E. Rodnyansky, A. G. Oliver, W.C. Boggess, J. Muldoon, Structure and compatibility of a magnesium electrolyte with a sulphur cathode, Nat. Commun. 2 (2011) 1–6.
[9] Y. Li, S. Guan, H. Huo, Y. Ma, Y. Gao, P. Zuo, G. Yin, A Review of Magnesium Aluminum Chloride Complex Electrolytes for Mg Batteries, Adv. Funct Mater. 31 (2021), 2100650.
[10] B. Li, R. Masse, C. Liu, Y. Hu, W. Li, G. Zhang, G. Cao, Kinetic surface control for improved magnesium-electrolyte interfaces for magnesium ion batteries, Energy Storage Mater. 22 (2019) 96–104.
[11] X. Li, T. Gao, F. Han, Z. Ma, X. Fan, S. Hou, N. Eidson, W. Li, C. Wang, Reducing Mg anode overpotential via ion conductive surface layer formation by iodine additive, Adv. Energy Mater. 8 (2018), 1701728.
[12] R.E. Doe, R. Han, J. Hwang, A.J. Gmitter, I. Shterenberg, H.D. Yoo, N. Pour, D. Aurbach, Novel, electrolyte solutions comprising fully inorganic salts with high anodic stability for rechargeable magnesium batteries, Chem. Comm. 50 (2013) 243–245.
[13] W.F. Li, S. Cheng, J. Wang, Y.C. Qiu, Z.Z. Zheng, H.Z. Lin, S. Nanda, Q. Ma, Y. Xu, F.M. Ye, M.N. Liu, L.S. Zhou, Y.G. Zhang, Synthesis, Crystal Structure, and Electrochemical Properties of a Simple Magnesium Electrolyte for Magnesium/Sulfur Batteries, Angew. Chem. Int. Edit 55 (2016) 6406–6410.
[14] Y. Li, P. Zuo, N. Zhang, X. Yin, R. Li, M. He, H. Huo, Y. Ma, C. Du, Y. Gao, Improving electrochemical performance of rechargeable magnesium batteries with conditioning-free Mg-Cl complex electrolyte, Chem. Eng. J. 403 (2021), 126398.
[15] J.H. Ha, B. Lee, M. Lee, T. Yim, S.H. Oh, Al-compatible boron-based electrolytes for rechargeable magnesium batteries, Chem. Comm. 56 (2020) 14163–14166.
[16] H.M. Xu, Z.H. Zhang, Z.L. Cui, A.B. Du, C.L. Lu, S.M. Dong, J. Ma, X.H. Zhou, G. L. Cui, Strong anion receptor-assisted boron-based Mg electrolyte with wide electrochemical window and non-nucleophilic characteristic, Electrochem. Commun. 83 (2017) 72–76.
[17] Z.H. Zhang, Z.L. Cui, L.X. Qiao, J. Guan, H.M. Xu, X.G. Wang, P. Hu, H.P. Du, S. Z. Li, X.H. Zhou, S.M. Dong, Z.H. Liu, G.L. Cui, L.Q. Chen, Novel Design Concepts of Efficient Mg-Ion Electrolytes toward High-Performance Magnesium-Selenium and Magnesium-Sulfur Batteries, Adv. Energy Mater. 7 (2017), 1602055.
[18] Z. Zhao-Karger, M.E.G. Bardaji, O. Fuhr, M. Fichtner, A new class of non-corrosive, highly efficient electrolytes for rechargeable magnesium batteries, J. Mater. Chem. A 5 (2017) 10815–10820.
[19] T. Mandai, Critical Issues of Fluorinated Alkoxyborate-Based Electrolytes in Magnesium Battery Applications, ACS Appl. Mater. Interfaces 12 (2020) 39135–39144.
[20] K. Tang, A. Du, S. Dong, Z. Cui, X. Liu, C. Lu, J. Zhao, X. Zhou, G. Cui, A Stable Solid Electrolyte Interphase for Magnesium Metal Anode Evolved from a Bulky Anion Lithium Salt, Adv. Mater. (2019), 1904987.
[21] V. Bhaghavathi Parambath, Z. Zhao-Karger, T. Diemant, M. Jäckle, Z. Li, T. Scherer, A. Gross, R.J. Behm, M. Fichtner, Investigation on the formation of Mg metal anode/electrolyte interfaces in Mg/S batteries with electrolyte additives, J. Mater. Chem. A 8 (2020) 22998–23010.
[22] Z. Zhao-Karger, R.Y. Liu, W.X. Dai, Z.Y. Li, T. Diemant, B.P. Vinayan, C.B. Minella, X.W. Yu, A. Manthiram, R.J. Behm, M. Ruben, M. Fichtner, Toward Highly Reversible Magnesium-Sulfur Batteries with Efficient and Practical Mg[B(hfip)(4)](2) Electrolyte, Acs Energy Lett. 3 (2018) 2005–2013.
[23] I. Shterenberg, M. Salama, H.D. Yoo, Y. Gofer, J.-B. Park, Y.-K. Sun, D. Aurbach, Evaluation of (CF3SO2) 2N−(TFSI) based electrolyte solutions for Mg batteries, J. Electrochem. Soc. 162 (2015) A7118–A7128.
[24] T. Gao, S. Hou, F. Wang, Z. Ma, X. Li, K. Xu, C. Wang, Reversible S0/MgSx Redox Chemistry in a MgTFSI2/MgCl2/DME Electrolyte for Rechargeable Mg/S Batteries, Angewandte Chemie 129 (2017) 13711–13715.
[25] Y.Y. Yang, Y.X. Qiu, Y.N. NuLi, W.Q. Wang, J. Yang, J.L. Wang, A novel magnesium electrolyte containing a magnesium bis(diisopropyl)amide-magnesium chloride complex for rechargeable magnesium batteries, J. Mater. Chem. A 7 (2019) 18295–18303.
[26] Y. Bi, S. He, C. Fan, J. Luo, B. Yuan, T.L. Liu, A robust ionic liquid magnesium electrolyte enabling Mg/S batteries, J. Mater. Chem. A 8 (2020) 12301–12305.
[27] Z. Zhao-Karger, X.Y. Zhao, D. Wang, T. Diemant, R.J. Behm, M. Fichtner, Performance Improvement of Magnesium Sulfur Batteries with Modified Non-Nucleophilic Electrolytes, Adv. Energy Mat. 5 (2015), 1401155.
[28] S.B. Son, T. Gao, S.P. Harvey, K.X. Steirer, A. Stokes, A. Norman, C. Wang, A. Cresce, K. Xu, C. Ban, An artificial interphase enables reversible magnesium chemistry in carbonate electrolytes, Nat. Chem. 10 (2018) 532–539.
[29] Y. Li, P. Zuo, R. Li, H. Huo, Y. Ma, C. Du, Y. Gao, G. Yin, R.S. Weatherup, Formation of an Artificial Mg(2+)-Permeable Interphase on Mg Anodes Compatible with Ether and Carbonate Electrolytes, ACS Appl. Mater. Interfaces 13 (2021) 24565–24574.
[30] M. Song, J. Niu, H. Gao, T. Kou, Z. Wang, Z. Zhang, Phase engineering in lead–bismuth system for advanced magnesium ion batteries, J. Mater. Chem. A 8 (2020) 13572–13584.
[31] R. Li, Y. Li, R. Zhang, M. He, Y. Ma, H. Huo, P. Zuo, G. Yin, Voltage hysteresis of magnesium anode: Taking magnesium-sulfur battery as an example, Electrochim. Acta 369 (2021), 137685.
[32] D.J. Wetzel, M.A. Malone, R.T. Haasch, Y. Meng, H. Vieker, N.T. Hahn, A. Gölzhäuser, J.M. Zuo, K.R. Zavadil, A.A. Gewirth, R.G. Nuzzo, Passivation Dynamics in the Anisotropic Deposition and Stripping of Bulk Magnesium Electrodes During Electrochemical Cycling, ACS Appl. Mater. Interfaces 7 (2015) 18406–18414.
[33] S.Y. Ha, Y.W. Lee, S.W. Woo, B. Koo, J.S. Kim, J. Cho, K.T. Lee, N.S. Choi, Magnesium(II) bis(trifluoromethane sulfonyl) imide-based electrolytes with wide electrochemical windows for rechargeable magnesium batteries, ACS Appl. Mater. Interfaces 6 (2014) 4063–4073.
[34] T. Gao, M. Noked, A.J. Pearse, E. Gillette, X. Fan, Y. Zhu, C. Luo, L. Suo, M. A. Schroeder, K. Xu, S.B. Lee, G.W. Rubloff, C. Wang, Enhancing the reversibility of Mg/S battery chemistry through Li(+) mediation, J. Am. Chem. Soc. 137 (2015) 12388–12393.
[35] X. Yu, A. Manthiram, Performance Enhancement and Mechanistic Studies of Magnesium–Sulfur Cells with an Advanced Cathode Structure, ACS Energy Lett. 1 (2016) 431–437.
[36] A.B. Du, Z.H. Zhang, H.T. Qu, Z.L. Cui, L.X. Qiao, L.L. Wang, J.C. Chai, T. Lu, S. M. Dong, T.T. Dong, H.M. Xu, X.H. Zhou, G.L. Cui, An efficient organic magnesium borate-based electrolyte with non-nucleophilic characteristics for magnesium-sulfur battery, Energ Environ. Sci. 10 (2017) 2616–2625.
[37] H. Du, Z. Zhang, J. He, Z. Cui, J. Chai, J. Ma, Z. Yang, C. Huang, G. Cui, A Delicately Designed Sulfide Graphdiyne Compatible Cathode for High-Performance Lithium/Magnesium-Sulfur Batteries, Small 13 (2017), 1702277.
[38] A. Robba, A. Vizintin, J. Bitenc, G. Mali, I. Arcon, M. Kavcic, M. Zitnik, K. Bucar, G. Aquilanti, C. Martineau-Corcos, A. Randon-Vitanova, R. Dominko, Mechanistic Study of Magnesium-Sulfur Batteries, Chem. Mater. 29 (2017) 9555–9564.
[39] T. Gao, S. Hou, K. Huynh, F. Wang, N. Eidson, X. Fan, F. Han, C. Luo, M. Mao, X. Li, C. Wang, Existence of Solid Electrolyte Interphase in Mg Batteries: Mg/S Chemistry as an Example, ACS Appl. Mater. Interfaces 10 (2018) 14767–14776.
[40] Y. Xu, W. Li, G. Zhou, Z. Pan, Y. Zhang, A non-nucleophilic mono-Mg2+ electrolyte for rechargeable Mg/S battery, Energy Storage Mater. 14 (2018) 253–257.
[41] X. Zhou, J. Tian, J. Hu, C. Li, High Rate Magnesium-Sulfur Battery with Improved Cyclability Based on Metal-Organic Framework Derivative Carbon Host, Adv. Mater. 30 (2018), 1704166.
[42] D. Huang, S. Tan, M. Li, D. Wang, C. Han, Q. An, L. Mai, Highly Efficient Non-Nucleophilic Mg(CF3SO3)2-Based Electrolyte for High-Power Mg/S Battery, ACS Appl. Mater. Interfaces 12 (2020) 17474–17480.
[43] J. Hacker, C. Danner, B. Sievert, I. Biswas, Z. Zhao-Karger, N. Wagner, K. A. Friedrich, Investigation of Magnesium-Sulfur Batteries using Electrochemical Impedance Spectroscopy, Electrochim. Acta 338 (2020), 135787.
[44] Y. Xu, Y. Ye, S. Zhao, J. Feng, J. Li, H. Chen, A. Yang, F. Shi, L. Jia, Y. Wu, X. Yu, P. A. Glans-Suzuki, Y. Cui, J. Guo, Y. Zhang, Situ X-ray Absorption Spectroscopic Investigation of the Capacity Degradation Mechanism in Mg/S Batteries, Nano Lett. 19 (2019) 2928–2934.
[45] B.P. Vinayan, H. Euchner, Z. Zhao-Karger, M.A. Cambaz, Z. Li, T. Diemant, R. J. Behm, A. Gross, M. Fichtner, Insights into the electrochemical processes of rechargeable magnesium–sulfur batteries with a new cathode design, J. Mater. Chem. A 7 (2019) 25490–25502.
[46] Z. Meng, D. Foix, N. Brun, R. Dedryvère, L. Stievano, M. Morcrette, R. Berthelot, Alloys to Replace Mg Anodes in Efficient and Practical Mg-Ion/Sulfur Batteries, ACS Energy Lett. 4 (2019) 2040–2044.
[47] Y. Li, P. Zuo, R. Li, M. He, Y. Ma, Y. Shi, X. Cheng, C. Du, G. Yin, Electrochemically-driven interphase conditioning of magnesium electrode for magnesium sulfur batteries, J. Energy Chem. 37 (2019) 215–219.
[48] D. Allison, G. Johansson, C. Allan, U. Gelius, H. Siegbahn, J. Allison, K. Siegbahn, Molecular spectroscopy by means of ESCA: V. Boron compounds, J. Electron Spectrosc. Relat. Phenom. 1 (1972) 269–283.
[49] P.C. Howlett, N. Brack, A.F. Hollenkamp, M. Forsyth, D.R. Macfarlane, Characterization of the lithium surface in N-methyl-N-alkylpyrrolidinium bis (trifluoromethanesulfonyl) amide room-temperature ionic liquid electrolytes, J. Electrochem. Soc. 153 (2006) A595.